Sustainable Energy & Fuels

ROYAL SOCIETY OF CHEMISTRY

PAPER

View Article Online
View Journal | View Issue

Cite this: *Sustainable Energy Fuels*, 2021, **5**, 3847

Isomerization of glucose to fructose catalyzed by metal–organic frameworks

Marta Lara-Serrano, [a] Silvia Morales-delaRosa, *[a] Jose M. Campos-Martin, *[a] Víctor K. Abdelkader-Fernández, [b] Luís Cunha-Silva [b] and Salete S. Balula [b]

The isomerization reaction of glucose to fructose was studied using five selected metal–organic frameworks (MOFs) as catalysts and a mixture of γ-valerolactone and 10% H_2O as solvent. MOFs with different metal cations (Cr^{3+}, Al^{3+}, Cu^{2+}, and Fe^{3+}) were tested between 100 and 140 °C. The activity tests show that the MOF with chromium yields a higher amount of fructose. A comparison between MIL-101(Cr) and MIL-53(Cr) shows a higher yield of fructose with MIL-101(Cr) (23% at 140 °C) in a short reaction time, due to the higher pore size of the MOF structure. The stability of this catalyst was confirmed, and it could be recycled 5 times without a significant loss of activity and exhibited an excellent fructose yield of 23–35% after 1 h of the reaction. In this work, the superior results found are due to the large porous MIL-101(Cr) catalyst combined with aprotic solvents (γ-valerolactone–10% H_2O).

Received 20th May 2021
Accepted 11th June 2021

DOI: 10.1039/d1se00771h

rsc.li/sustainable-energy

Introduction

Fructose is a key intermediate derived from biomass to produce fuel and high value added chemical products. Numerous studies have revealed that it is easier to obtain 5-hydroxymethylfurfural (5-HMF) (Fig. 1), levulinic acid, lactic acid, *etc.* from fructose than from glucose.[1–3] Nevertheless, fructose is not abundant in nature; in contrast, glucose is quite abundant. In this context, the isomerization reaction of glucose to fructose appears to be the most suitable procedure to obtain fructose. The maximum glucose-to-fructose conversion in this process is limited by the thermodynamic equilibrium between these two isomeric compounds and will strongly depend on the specific reaction temperature.[2,3]

At present, fructose can be generated at a large scale in the production of corn syrup (HFCS), a high fructose sweetener. In this process, the reaction is catalyzed enzymatically,[1,2,4] and despite the high selectivity of this reaction, several drawbacks increase processing costs, including the slow kinetics of enzymatic reactions, the use of buffering solutions to maintain pH, narrow operating temperatures, and strict feed purification requirements. For this reason, interest in the use of chemical catalysis, which can avoid these drawbacks, has grown during the last several years.

Glucose isomerization to fructose can be catalyzed by basic catalysts according to the Lobry de Bruyn–Alberda van Ekenstein reaction[2,3,5–8] or by acid catalysts.[1,9–12] Among the latter, special attention has been paid to the use of Lewis acid catalysts,[1,9–12] such as metal chloride salts[13–16] and heterogeneous zeolite-based systems modified with Sn, Ti, or Zr.[9,17,18]

Metal–organic frameworks (MOFs), which act as Lewis acid catalysts, are very interesting candidates. MOFs are crystalline nanostructured materials composed of metal nodes and organic linkers that present high surface areas and well-defined pore systems. Furthermore, they have numerous modifiable compositions and can be easily functionalized, making them excellent and promising materials in heterogeneous catalysis applications, such as the oxidative desulfurization of fuels,[19,20] electrocatalysis,[21–24] gas adsorption and separation, hydrogen storage, drug delivery[25,26] and, in particular, catalytic and biomass valorization.[10,27–32] A few studies have evaluated the catalytic activity of MOFs in glucose isomerization.[10,33–35] But, the main effort has been devoted to modifying MOFs (*via* metal

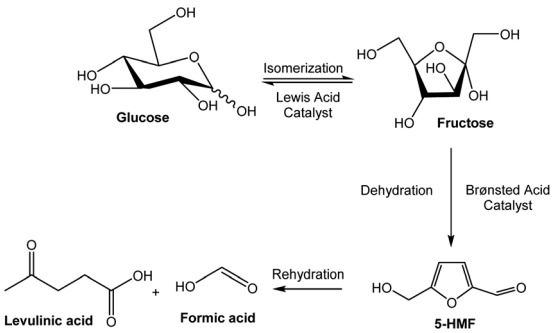

Fig. 1 Scheme of the catalyzed isomerization and dehydration of fructose from glucose and some of the compounds obtained from fructose by acid catalysis.

[a]*Grupo de Energía y Química Sostenible (EQS), Instituto de Catálisis y Petroleoquímica, CSIC, c/Marie Curie, 2 Cantoblanco, 28049 Madrid, Spain. E-mail: jm.campos@csic.es; smorales@icp.csic.es*

[b]*REQUIMTE/LAQV, Departamento de Química e Bioquímica, Faculdade de Ciências da Universidade do Porto, Rua do Campo Alegre, 4169-007 Porto, Portugal*

clusters or organic ligands) to be applied for the one-pot synthesis of 5-HMF from glucose.[36–39]

Apart from catalyst selection, another decisive factor in glucose-to-fructose isomerization is the employed solvent. Here, the first option is water[2,7–9,18,40] due to the good solubility of sugars in it, although various other solvents have been tested to improve the reaction rate and minimize the production of secondary products, such as alcohols,[5,11,41] ionic liquids,[42] and polar aprotic organic solvents including *N*,*N*-dimethylformamide (DMF), dimethyl sulfoxide (DMSO), dimethylacetamide (DMA), sulfolane, γ-valerolactone, acetone, and 1,4-dioxane.[4,43]

This work presents a novel study on the isomerization of glucose to fructose by using five selected MOF catalysts (three MOFs synthesized, MIL-53(Cr), CuBTC, and MIL-101(Cr), and two other commercial catalysts, FeBTC, and MIL-53(Al)). The utilization of different MOF-based catalysts with diverse porosities and Lewis acid sites in the form of metal cations (Cr^{3+}, Al^{3+}, Cu^{2+}, and Fe^{3+}) has allowed us to evaluate the influence of these parameters on their catalytic activity.

Experimental

Materials: reagents and solvents

All chemicals used in MOF preparation were used as received without further purification: chromium(III) nitrate nonahydrate (Panreac, 99%), benzene-1,4-dicarboxylic acid (Aldrich, 98%), hydrofluoric acid (Aldrich 40–45%), copper nitrate ($Cu(NO_3)_2 \cdot 3H_2O$, AR, Damao), 1,3,5-benzenetricarboxylic acid (H_3BTC, 99%, J&K), *N*,*N*-dimethylformamide (DMF, AR, Fuyu) and ethanol (EtOH, AR, Damao). Glucose, Basolite® F300 (FeBTC), Basolite® A100 (MIL-53(Al)), and γ-valerolactone (GVL, ≥99%) were acquired from Aldrich.

Catalyst preparation

Synthesis of MIL-53(Cr). The porous MOF material MIL-53(Cr), where MIL is the abbreviation for the Material of Institute Lavoisier, was hydrothermally prepared using traditional synthesis.[44] Initially, a mixture of chromium(III) nitrate (4 mmol), terephthalic acid (4 mmol), and hydrofluoric acid (4 mmol) in 20 mL of H_2O was stirred at room temperature. Then, the mixture was transferred to an autoclave and was heated at 220 °C for 72 h. After slowly cooling inside the oven, the resultant material was isolated by centrifugation and dried at 100 °C overnight.

Synthesis of CuBTC. First, copper hydroxide was prepared[45] by the addition of an aqueous solution of NaOH (1.0 M, 16.5 mL) into an aqueous $Cu(NO_3)_2 \cdot 3H_2O$ solution (2.0 g, 0.8 mmol, dissolved in 15 mL of deionized water). CuBTC was synthesized by mixing an ethanolic solution (38 mL) of trimesic acid (1.739 g, 0.8 mmol) with copper hydroxide solution. After 30 min of ultrasonic treatment, the color changed from light blue to dark blue. The solid was centrifuged, washed three times with ethanol, and dried.

Synthesis of MIL-101(Cr). The porous MOF material MIL-101(Cr), was hydrothermally prepared using an adaptation[19] of the original method.[46] Initially, a mixture of chromium(III) nitrate (2 mmol), terephthalic acid (2 mmol), and hydrofluoric acid (100 μL) in 10 mL of H_2O was stirred at room temperature. After obtaining a homogeneous suspension, the mixture was transferred to an autoclave and was heated at 220 °C for 9 h. After slowly cooling inside the oven, the resultant material was isolated by centrifugation and purified through double DMF treatment followed by double ethanol treatment.

Physicochemical characterization

Nitrogen adsorption. The textural properties of the MOFs were determined from nitrogen adsorption–desorption isotherms recorded at −196 °C with a Micromeritics TriStar 3000 apparatus. The samples were previously degassed at 200 °C for 24 h under vacuum (10^{-4} mbar) to ensure a clean dry surface free of any loosely bound adsorbed species. The specific areas of the samples were determined according to a standard BET procedure using N_2 adsorption data obtained in the relative equilibrium pressure interval of $0.03 < P/P_0 < 0.3$ and a value of 0.162 nm^2 for the cross-sectional area of an adsorbed nitrogen molecule.

Attenuated total reflection infrared spectroscopy (ATR-FTIR). The spectra of the solids were recorded with a PerkinElmer Spectrum BX system equipped with a PIKE Gladi ATR. A total of 180 cumulative scans were performed in attenuated total reflection mode with a resolution of 4 cm^{-1} in the frequency range of 4000–450 cm^{-1}.

Powder X-ray diffraction (PXRD). X-ray diffraction analyses were performed at Instituto de Física dos Materiais da Universidade do Porto, IFIMUP (Porto, Portugal). XRD patterns were obtained with a Rigaku SmartLab X-ray diffractometer using a CuKα X-ray source ($\lambda = 1.5418$ Å; acceleration potential = 45 kV; current = 200 mA). A Bragg–Brentano geometry was used. The samples were ground and placed on a stainless-steel plate, and data were recorded in steps over a range of Bragg angles (2θ) between 4° and 90° at a scanning rate of 0.02° per step and an accumulation time of 50 s.

Scanning electron microscopy (SEM). SEM micrographs of the different elements were collected at CEMUP (Porto, Portugal) using a high resolution (Schottky) environmental microscope and analysed with X-ray microanalysis and backscattered electron diffraction pattern analysis (FEI Quanta 400FEG/EDAX Genesis X4 M). Measurements were carried out under high-vacuum conditions.

Catalysis studies

Isomerization reaction. The catalytic tests were carried out in a Mettler-Toledo EasyMax 102© stirred glass tank reactor. First, 0.080 g of catalyst was added to 5 mL of a 1 wt% solution of glucose in 90 wt% GVL-10 wt% H_2O and mixed with a stirring magnet. After 15 min of temperature stabilization, the reaction began. For all catalysts, the reactions were tested periodically after 15, 30, 60, and 120 min using three different temperatures: 100, 120, and 140 °C. These analyses were performed by HPLC (Agilent Technologies HPLC 1200 and 1260 series). Chromatographic separation was performed with an HPLC 1200 chromatograph, a Hi-PLEX H column at 60 °C, 0.6

mL min^{-1} sulfuric acid aqueous solution (0.01 M) as the mobile phase, a refractive index detector, and an ultraviolet detector. On the other hand, chromatographic separation was performed with an HPLC 1260 chromatograph, a Hi-Plex Ca(Duo) column at 85 °C, a 0.6 mL min^{-1} water as the mobile phase for HPLC, and a refractive index detector. This method allows the analysis of sugars (glucose and fructose) and secondary products (5-hydroxymethylfurfural and furfural). Identification and quantification of the components were carried out by comparing the retention times and using internal calibration curves with reference compounds. All reaction tests were repeated at least three times, and the results are represented with error bars.

Recycling tests. For a typical catalytic reuse experiment, after a reaction cycle, the solid catalyst was collected from the reaction mixture *via* centrifugation and washed three times in GVL-10% H_2O, three times with water and once with acetone to facilitate drying. Then, the solid was dried in an oven at 50 °C overnight. Finally, this solid was used as the catalyst in the same reaction, as described in the preceding paragraphs.

Results and discussion

This work presents a study on the isomerization of glucose to fructose by using five selected MOF catalysts (three MOFs synthesized, MIL-53(Cr), CuBTC, and MIL-101(Cr), and two other commercial catalysts, FeBTC and MIL-53(Al)). The utilization of different MOF-based catalysts with diverse porosities and Lewis acid sites in the form of metal cations (Cr^{3+}, Al^{3+}, Cu^{2+}, and Fe^{3+}) has allowed us to evaluate the influence of these parameters on their catalytic activity. These reactions will take place in a mixture of 10% H_2O and γ-valerolactone (GVL).

In this study, two of these MOF catalysts (MIL-53(Cr) and MIL-53(Al)) have the same structure which consists of inorganic [metal–OH] chains formed by terephthalate-based linker molecules with a similar pore size structure. The metal center (Cr or Al) is octahedrally coordinated by six oxygen atoms. Four oxygen atoms come from different carboxylate groups and the remaining two atoms belong to two different μ-OH moieties, which bridge neighboring metal center.[47] The resulting structure contains one-dimensional-shaped pores. The CuBTC corresponds to the empirical formula $[Cu_3(BTC)_2(H_2O)_3]_n$ with interconnected $[Cu_2(O_2CR)_4]$ units (R = aromatic ring). The structure contains dimeric cupric tetracarboxylic secondary building units respectively with Cu–Cu separation. In the neutral network, twelve carboxylic oxygen atoms from the two BTC ligands are coordinated to four sites of each of the three Cu^{2+} ions.[48] Its iron counterpart, FeBTC, is constituted by iron building units where the iron in oxidation state Fe^{3+} is connected with BTC linkers,[49] however, the local environment around iron is still unknown. Finally, we compared the results with another MOF with a different structure and porous size, MIL-101(Cr), which is comprised of trimeric chromium(III) octahedral clusters interconnected by 1,4-benzenedicarboxylates.[50] MIL-101(Cr) has a larger pore size than the other MOFs studied.

Structural characterization

The region from 1400 to 1600 cm^{-1} in the ATR-FTIR spectra (Fig. 2) shows peaks attributed to the asymmetric and symmetric stretching vibration modes of the O–C–O framework. These peaks are present in all samples due to the presence of carboxylic groups in the framework links.[51] The other bands between 600 and 1600 cm^{-1} are attributed to benzene, including the stretching vibration (C=C) at 1508 cm^{-1} and deformation vibrations (C–H) at 1160, 1017, 884, and 750 cm^{-1}.[52] The MOF IR spectra exhibit some peaks attributed to the presence of the different metals: the CuBTC spectrum shows a vibration peak at 730 cm^{-1}, which might be attributed to the Cu–O stretching vibration, in which the oxygen atom is coordinated with Cu.[53] The FeBTC spectrum includes a characteristic band at 1109 cm^{-1} related to the metalorganic group C–O–Fe.[54] Regarding MIL-101(Cr), the moderate-intensity peak at 583 cm^{-1} can be ascribed to Cr–O stretching vibrations,[55] however, it is difficult to observe in the case of MIL-53(Cr) which has a spectrum similar to its aluminum counterpart. Finally, the spectrum of MIL-53(Al) shows a broad peak between 600 and 700 cm^{-1} assigned to asymmetric and symmetric O–Al–O stretching vibrations.[56] Thus, all characterization results indicate that the five MOF samples—prepared and commercial materials—present canonical structural arrangements corresponding to those referenced in the literature.

The PXRD patterns of all the MOFs studied match with those described in the literature (Fig. 3). The PXRD pattern of MIL-53(Cr) does not indicate complete crystallinity. Common peaks can be found with its chromium counterpart, MIL-

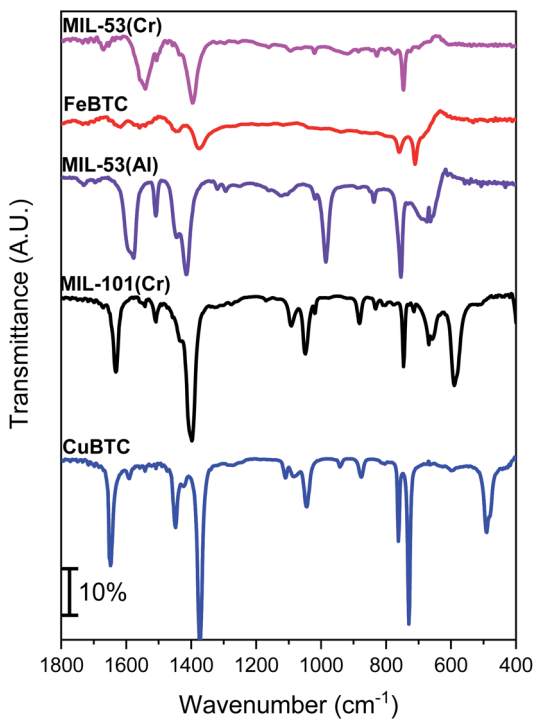

Fig. 2 ATR-FTIR spectra of the fresh MOFs used as catalysts in this study.

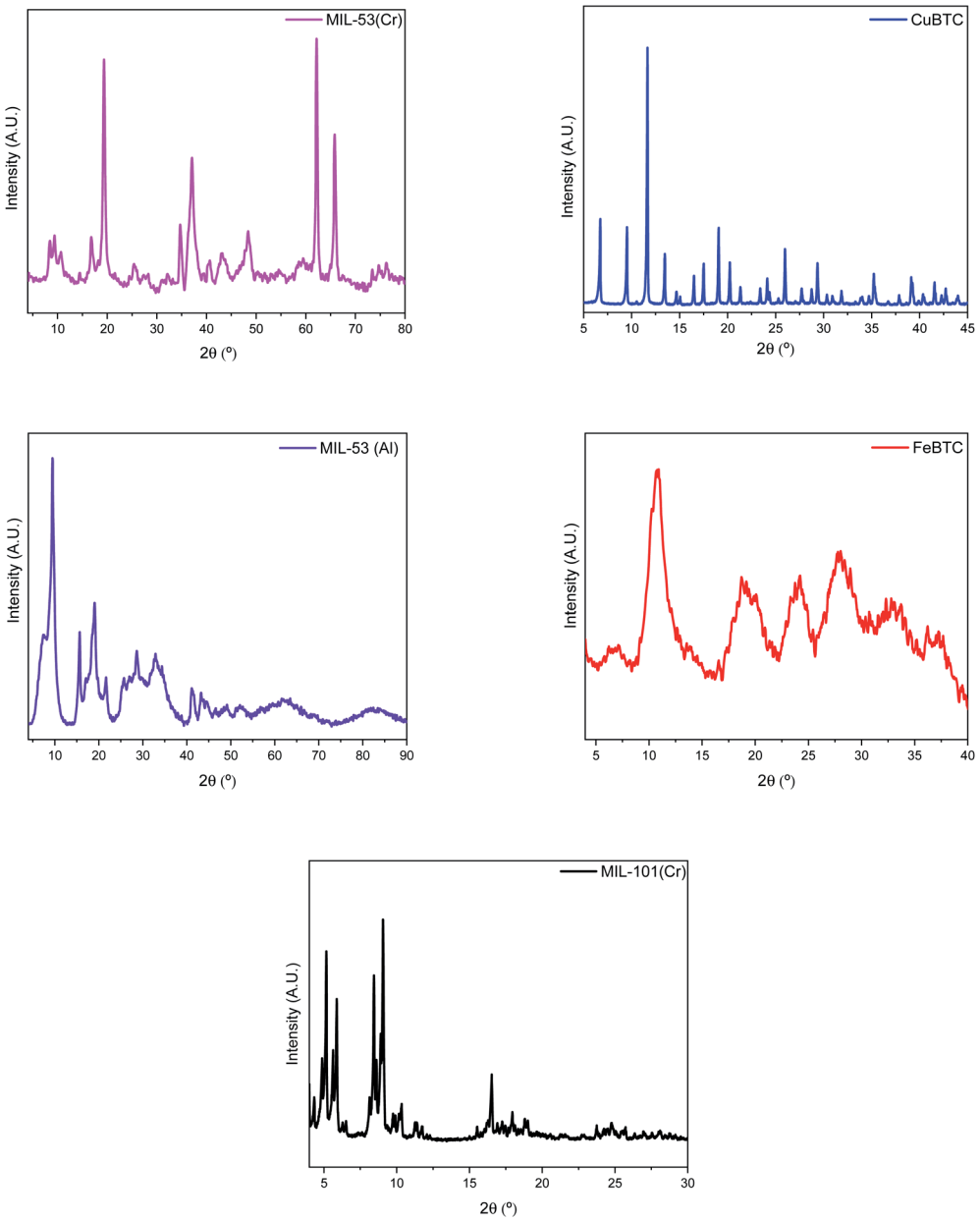

Fig. 3 PXRD patterns of all the MOF samples.

101(Cr), but of low intensity. This may be due to obtaining a mixed solid between MIL-101(Cr) and MIL-53(Cr), because the synthesis method is similar except for the number of hours (24 h *versus* 72 h respectively) that makes the crystal change, generating MIL-53(Cr). The PXRD pattern of CuBTC uniquely exhibits the presence of the CuBTC phase, with diffraction peaks identical to those described in previous studies.[57,58] Additionally, no impurities of Cu_2O are detected due to the absence of its characteristic diffraction peak at 36.4°.[45] The PXRD pattern of FeBTC shows peaks at Bragg angles of 10.9°, 18.8°, 24.2°, and 28.1°, which are typical of this structure.[59] The low-resolution diffraction pattern of FeBTC is a consequence of the semi-amorphous nature of this material. The X-ray diffraction pattern of reference sample MIL-53(Al) is consistent with previously published powder XRD data.[60] Finally, the PXRD patterns of synthesized MIL-101(Cr) presents a set of diffraction peaks at Bragg angles of 2.82°, 3.3°, 3.35°, 3.98°, 4.34°, 4.88°, 5.17°, 5.63°, 5.88°, 8.44°, and 9.62°, which corresponds to the MIL-101(Cr) framework.[61] SEM analysis was performed to check the correct synthesis of prepared MOFs (Fig. 4). On the one hand, the SEM micrographs of MIL-53(Cr) (Fig. 4a and b) show crystals of different sizes and shapes that present aggregates in their structure. The SEM images of CuBTC (Fig. 4c and d) show octahedral particles with sizes in the range of 200–500 nm and some aggregates. These results show the morphology in the published SEM images.[62] The SEM micrographs of the MIL-101(Cr) crystals (Fig. 4e and f) also show the presence of octahedral particles with smooth surfaces and sharp edges.

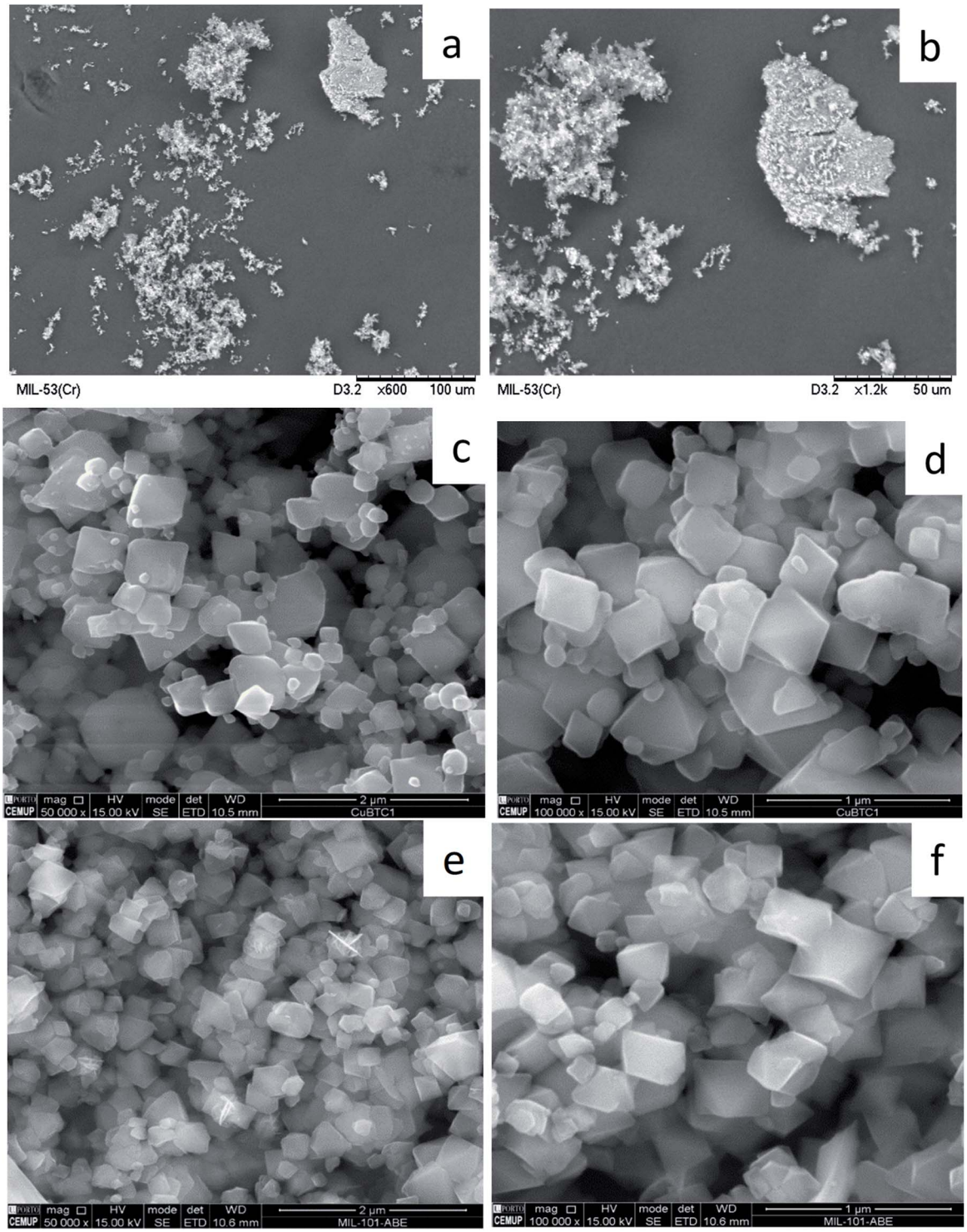

Fig. 4 SEM micrographs of (a and b) MIL-53(Cr), (c and d) CuBTC and (e and f) MIL-101(Cr).

However, these particles are not uniform in size, existing as diverse aggregates with sizes of approximately 120–250 nm.[63]

The textural parameters of the studied MOFs (Table 1) reveal large surface areas in all five cases, presenting similar values to those described in the literature. MIL-53(Cr), CuBTC, FeBTC, and MIL-53(Al) have increased and similar specific surface areas of ~1200 $m^2\ g^{-1}$, while the surface area of MIL-101(Cr) is the highest: 2187 $m^2\ g^{-1}$. A similar trend is followed for the MOF pore volumes (Table 1).

These differences can be attributed to the differences in the MOF structures and channel sizes. The largest channel size is 1.2 nm for MIL-101(Cr),[33] which corresponds to the largest surface area, while the channels of ~0.9 nm for MIL-53(Cr), CuBTC, FeBTC, and MIL-53(Al)[64–66] result in lower surface areas.

Table 1 Textural properties of MOFs determined from the corresponding nitrogen adsorption–desorption isotherms at −196 °C

MOF	BET surface area ($m^2\ g^{-1}$)	Pore volume ($cm^3\ g^{-1}$)
MIL-53(Cr)	1192	0.64
CuBTC	1277	0.61
MIL-53(Al)	1173	0.55
FeBTC	1254	0.55
MIL-101(Cr)	2187	1.15

Catalytic activity for glucose-to-fructose isomerization

The structures described with different metal centers were tested as catalysts for the glucose isomerization to fructose process. This reaction was studied at different temperatures between 100 and 140 °C. As expected, increasing the reaction temperature clearly increases the conversion of glucose and fructose yields (Fig. 5 and 6, respectively) for all the catalysts. However, the magnitudes of the catalytic activity improvement are different for each case: MIL-53(Cr) and FeBTC being the most active catalysts while MIL-53(Al) being the least active. The glucose conversion is always lower than 40% at 100 °C for all catalysts, reaching very similar final conversion percentages in the cases of CuBTC, MIL-53(Al), and FeBTC. The increases in reaction temperature enlarged the differences between the MOF catalytic activity levels, exhibiting significant differences at 140 °C. In addition, the shapes of the conversion profiles are quite different among the catalysts employed at 140 °C.

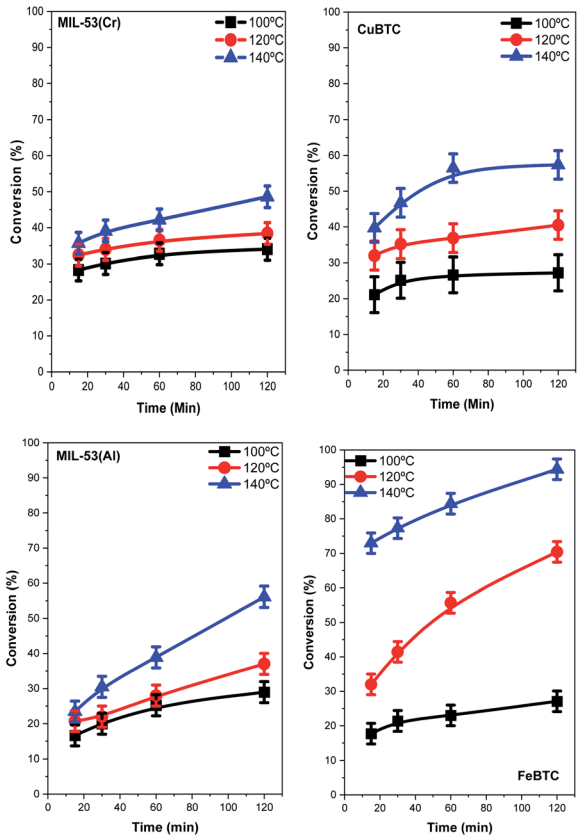

Fig. 5 Glucose conversion *versus* the reaction time for the isomerization of glucose to fructose catalysed by the four MOF samples.

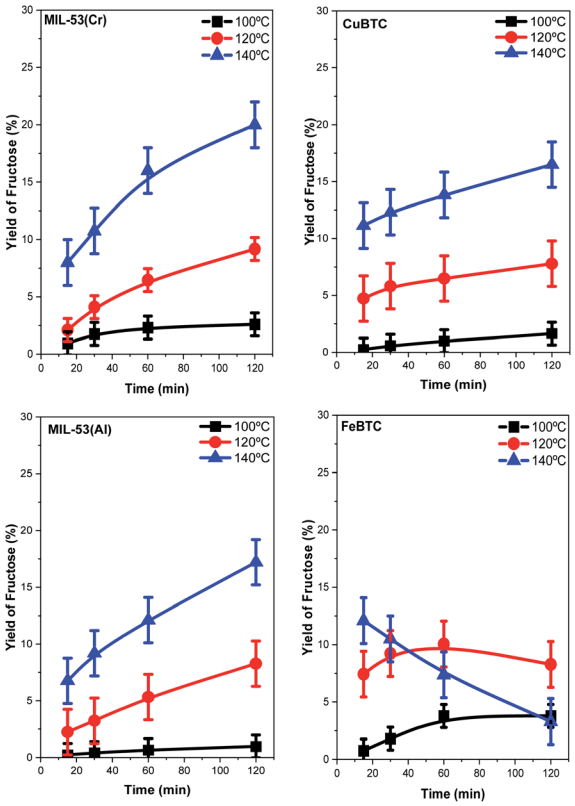

Fig. 6 Yield of fructose obtained in the isomerization of glucose to fructose by using each MOF catalyst *versus* time.

The conversion of glucose increases continuously with time during the whole experiment with MIL-53(Cr), MIL-53(Al), and FeBTC catalysts. Using the latter catalyst, the conversion value after the first 15 min of the reaction is already approximately 75%. In fact, the highest conversion of 93% was obtained using the FeBTC catalyst after 2 h of the reaction. The formation of fructose was investigated with a blank experiment, *i.e.*, without the presence of a catalyst, and in this case, no fructose formed (result not shown). In the presence of MOF catalysts, fructose yields increase with increasing reaction temperature, except when using the FeBTC catalyst. Using FeBTC, a low yield of fructose is detected, especially at 140 °C (increasing from 12.5% at 15 min to 3% after 2 h), despite the high conversion obtained. FeBTC exhibits a different behavior from the other MOFs studied since its fructose yield profiles show a maximum value after the first hour of the reaction which diminished monotonically from the first to the second hour of the process. This result is in contrast with the high conversion of glucose observed.

The high conversion and low fructose yield can be related to the redox properties of Fe^{3+}, because as has already been reported, starch, cellulose, and glucose could be oxidized to CO_2 by a Fe^{3+} catalyst,[67] and this effect is more evident at higher

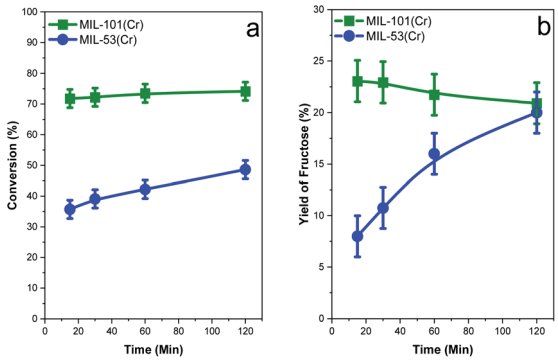

Fig. 7 Comparison of conversion (a) and the fructose yield (b) obtained for the MIL-53(Cr) and MIL-101(Cr) catalysts at 140 °C for different reaction times.

temperatures (140 °C). Regarding the other MOFs, the fructose yield can be related to the Lewis acid properties of the metal present in the MOF structure and their interaction with glucose; several studies have shown that chromium and aluminum salts are active in glucose isomerization, but the most active catalysts are based on chromium.[13,68,69] The yield of fructose follows a trend similar to that previously observed with homogenous chloride salts in solution.[14,40] The best results are shown with the MIL-53(Cr) catalysts; a 20% of fructose yield is obtained after two hours of reaction at 140 °C.

Due to the interesting activity results obtained with the MIL-53(Cr) catalyst for the isomerization of glucose to fructose, we chose to use MIL-101(Cr) in this reaction because this MOF has a larger pore size owing to its different structure. The comparison of the fructose conversion and yield is shown in Fig. 7. Both MOFs are active in the reaction. MIL-53(Cr) shows an increase of conversion with the reaction time; however, MIL-101(Cr) shows a small increase in conversion up to 30 minutes, remaining constant for long reaction times. The conversion level of MIL-101(Cr) is clearly higher than that of MIL-53(Cr). The fructose yield profiles showed a different profile between catalysts. At short reaction times, the MIL-101(Cr) catalyst shows a maximum yield of around 23% decreasing slightly at longer reaction times. However, the MIL-53(Cr) catalyst showed an increase in fructose yield with the reaction time. The formation of small amounts of anhydrofructose and anhydroglucose is detected and also the amount of 5-HMF and furfural in all cases was pretty small; then the main by-products formed in the reaction are humins.

The catalytic system (catalyst and solvent) reaches high glucose conversion and fructose yield in comparison with similar catalysts, reaching similar performance to optimized Sn-containing Lewis acidic zeolites. A comparison of our results with others systems used in the bibliography is compiled in Table 2. The catalytic activity and the fructose yield obtained in this work are notably higher than the values previously reported for the same catalysts (see entries 4–7 of Table 2); in this work, very fast conversion is reached in only 15–30 min instead of the much longer 8–24 h period described in previous studies.[33] These improvements must be related to the catalysts used and the selected solvents.

Given the results and the difficulty to compare our results with those previously published, we tested MIL-101(Cr) at different temperatures (100, 120, 130, and 140 °C) during 30 minutes of reaction using GVL-10% H_2O as solvent (Fig. 8). In addition, for comparative purposes, MIL-101(Cr) was tested at 130 °C for 30 minutes but using water as a solvent. The results show that for the same reaction time, using GVL-10% H_2O as solvent, glucose conversion and fructose yield increase with increasing temperature. At 130 °C, the fructose yield is about 10% in 30 minutes, indicating a higher activity than previous reports.[34] The use of GVL-10% H_2O as solvent enhances the catalytic activity compared to the use of only water (Fig. 8). These results show that not only the catalyst is important but also the choice of solvent is. Numerous studies have focused on glucose isomerization employing protic solvents; however, in this work, we utilized a nonprotic solvent (γ-valerolactone).

The reaction mechanism of glucose isomerization on Lewis acid sites has been studied by several authors, showing that intra-hydride transfer (C2 to C1) was the dominant reaction pathway in heterogeneous and homogenous systems.[4,9,35,40] The use of protic or nonprotic solvents has a strong effect on the balance of Lewis and Brønsted acid sites in the catalyst;[27] thus, protic solvents generate Brønsted acid sites due to solvent molecules being ligated to metal atoms.[27] As a consequence, the use of a nonprotic solvent in this study favors the proliferation of Lewis acid sites, which are very active for the glucose isomerization reaction.

Catalyst recycling capacity

The activity results have shown that MIL-101(Cr) is the most efficient catalyst for the glucose-to-fructose isomerization reaction, with glucose conversion and fructose yield values always

Table 2 Recompilation of glucose isomerization activity results described in the literature and comparison with this work

Catalyst and solvent	T (°C)	Time	Glucose conv. (%)	Fructose yield (%)	Ref.
Sn-β/water	140	12 h	46	30	1
Zr-MOF-808/water	140	30 min	35	5.4	35
UiO-66(Zr)/water	140	30 min	20	7.2	35
MIL-101(Cr) nano/water	100	24 h	46	25	10
MIL-101(Cr)/water	100	24 h	22	12.6	33
MIL-101(Cr)/water	130	8 h	28	20	34
MIL-101(Cr)/GVL-water	140	30 min	70	23	This work

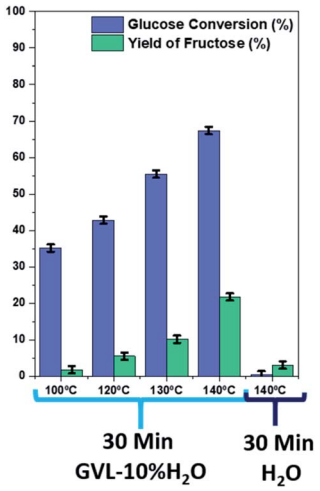

Fig. 8 Comparison of results obtained for glucose conversion and fructose yield using GVL-H_2O and water as solvent. Reaction conditions: 5 mL of 1 wt% glucose in GVL-10% H_2O, 0.080 g of catalyst, different temperatures and a reaction time 30 min.

above 70% and 23%, respectively, at 140 °C. For this reason, the stability and the recycling capacity of MIL-101(Cr) were investigated. The catalyst was reused for five consecutive reaction cycles lasting 1 h at 140 °C (the reaction time needed to reach the maximum conversion of glucose Fig. 9a).

After each cycle, the catalyst was recovered by centrifugation, and the solid obtained after the reaction was collected and washed three times in GVL-10% H_2O, three times with water and once with acetone to facilitate drying. Then, it was dried at 50 °C overnight in an oven.

Although the conversion level decreases slightly from the original reaction to the first reuse cycle (Fig. 8a), this value is maintained for 5 reuse cycles. The fructose yield increases from 23 to 28% after the first reuse cycle and then becomes close to 35% in the subsequent reuses. These data indicate that MIL-101(Cr) is an effective catalyst for glucose-to-fructose

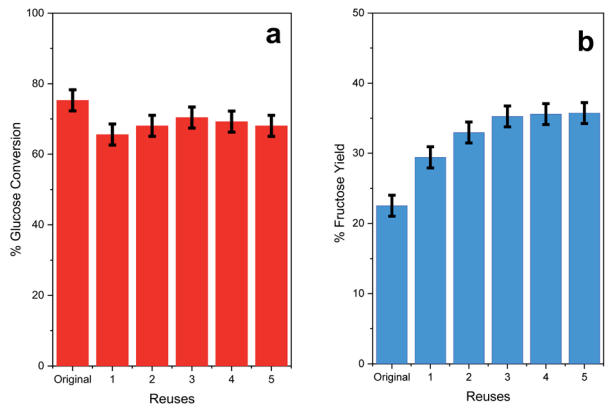

Fig. 9 (a) Conversion of glucose and (b) fructose yield after several reuses of MIL-101(Cr) used as the catalyst. Reaction conditions: 5 mL of 1 wt% glucose in 10 wt% H_2O-90 wt% GVL, 0.080 g of catalyst, T = 140 °C, and a reaction time of 1 h.

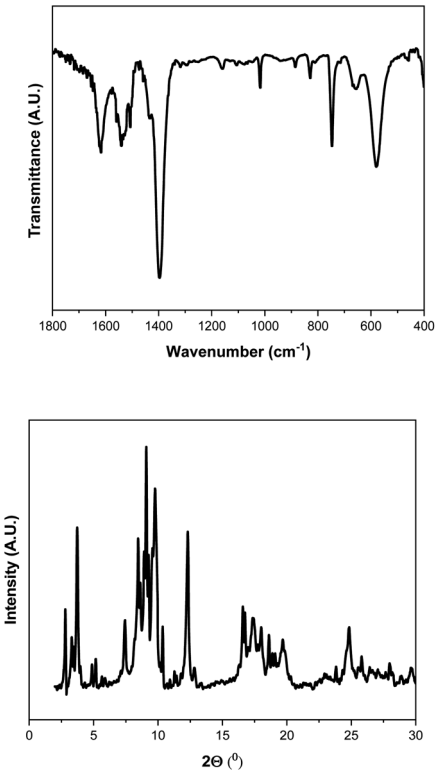

Fig. 10 ATR-FTIR spectrum (top) and PXRD pattern (bottom) of MIL-101(Cr) after five uses.

isomerization and can be reused in various consecutive reactions. The catalyst MIL-101(Cr) after being reused for five catalytic cycles was characterized by PXRD, IR, and SEM, demonstrating its robustness and stability (Fig. 9 and 10). In fact, the characteristic features of the diffraction patterns and the vibrational bands of MIL-101(Cr) are present in the sample after catalytic reuse, suggesting that the global crystalline structure of the MOF material was maintained. However, some small modifications can be found in the diffraction pattern and IR spectrum (Fig. 10), and the morphology of the particles after catalytic tests (SEM images, Fig. 11) differed from the initial MOF structure (Fig. 2–4). This must be related to internal rearrangements that can occur in the MIL-101(Cr) framework after several consecutive catalytic processes and are promoted by the interactions of substrates and products with the MOF

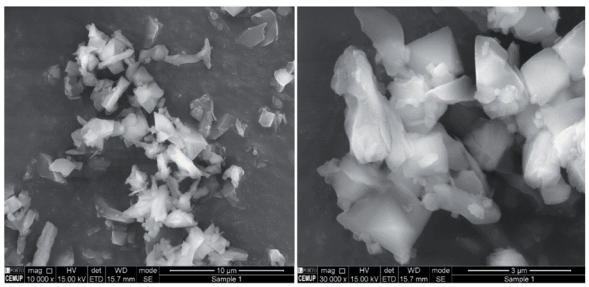

Fig. 11 SEM micrographs of MIL-101(Cr) after five uses.

structure. The remarkable increase in the fructose yield can be related to the presence of adsorbed water in the fresh catalyst pore structure due to its substantial hygroscopic characteristic. The presence of water in the fresh catalyst was proven based on the presence of the intense band at 1610 cm^{-1}, which is attributed to adsorbed molecular water bending (Fig. 2), and the intensity of this band is clearly reduced in the reused sample (Fig. 9). During the reaction, the catalyst undergoes a drying process due to the use of the GVL solvent; then, the water absorbed inside the catalyst is gradually removed during the reaction, and the amount of water adsorbed decreases after each reuse.

Conclusions

The catalysis of the isomerization reaction of glucose to fructose has been tested with five different MOF catalysts. We have demonstrated that these MOFs can catalyze this process in a GVL-10% H_2O medium. The results found in this work indicate that MOF catalysts combined with aprotic solvents produce a high conversion of glucose and a fructose formation rate in comparison with other studies that employ water or alcohols as solvent.

The activity results show that glucose conversion increases with increasing temperature for all the catalysts. In catalysts with the same structure, it is observed that FeBTC has the highest conversion (above 70%) while MIL-53(Cr) has the best fructose yield. When MIL-53(Cr) is compared to its chromium counterpart (MIL-101(Cr)) with a higher pore size, the profile shows an increase in fructose yield at early reaction times. Thus, MIL-101(Cr) is the catalyst that showed the highest fructose yield at 140 °C (~23%) in GVL-10% H_2O among the MOFs studied. The recycling capacity of MIL-101(Cr) was confirmed by performing 5 reuse reaction cycles; no significant loss in activity was observed, and the reaction with MIL-101(Cr) exhibited an increase in the fructose yield from 23 to 35% after 1 h of the reaction. The catalytic activity and yield of fructose achieved in this work are notably higher than those previously reported since we reached very high conversion and fructose yield values after 1 h of the reaction instead of the 8–24 h reaction reported in previous studies (Table 2), reaching similar performance to optimized Sn-containing Lewis acidic zeolites. The superior results found in this work are due to the large porous MIL-101(Cr) catalyst combined with aprotic solvents.

Author contributions

M. Lara-Serrano: investigation, formal analysis, and writing-original draft preparation. S. Morales-delaRosa: formal analysis, supervision, writing-reviewing, and editing. J. M. Campos-Martin: conceptualization, supervision, writing-reviewing and editing, project administration, funding acquisition. Víctor K. Abdelkader-Fernández: investigation, formal analysis. Luís Cunha-Silva: writing-reviewing and editing. Salete S. Balula: supervision, writing-reviewing, and editing, project administration, funding acquisition.

Conflicts of interest

There are no conflicts to declare.

Acknowledgements

This work was supported by the Comunidad de Madrid (Spain) and ERDF (European Regional Development Fund), grant number S2018/EMT-4344 (BIOTRES-CM). In addition, this work was supported by the projects REQUIMTE-LAQV (UIDB/50006/2020) and GlyGold PTDC/CTM-CTM/31983/2017 and the R&D project POCI-01-0145-FEDER-016422 – UniRCell, which was financed by national funds through the FCT/MCTES (Fundação para a Ciência e a Tecnologia/Ministerio de Ciências, Tecnologia e Ensino Superior). We acknowledge the support for the publication fee by the CSIC Open Access Publication Support Initiative through its Unit of Information Resources for Research (URICI).

Notes and references

1 M. Moliner, Y. Román-Leshkov and M. E. Davis, *Proc. Natl. Acad. Sci. U. S. A.*, 2010, **107**, 6164–6168.
2 A. A. Marianou, C. M. Michailof, A. Pineda, E. F. Iliopoulou, K. S. Triantafyllidis and A. A. Lappas, *ChemCatChem*, 2016, **8**, 1100–1110.
3 A. A. Marianou, C. M. Michailof, D. K. Ipsakis, S. A. Karakoulia, K. G. Kalogiannis, H. Yiannoulakis, K. S. Triantafyllidis and A. A. Lappas, *ACS Sustainable Chem. Eng.*, 2018, **6**, 16459–16470.
4 I. Delidovich and R. Palkovits, *ChemSusChem*, 2016, **9**, 547–561.
5 M. Yabushita, N. Shibayama, K. Nakajima and A. Fukuoka, *ACS Catal.*, 2019, **9**, 2101–2109.
6 C. Moreau, R. Durand, A. Roux and D. Tichit, *Appl. Catal., A*, 2000, **193**, 257–264.
7 M. Ventura, J. A. Cecilia, E. Rodríguez-Castellón and M. E. Domine, *Green Chem.*, 2020, **22**, 1393–1405.
8 S. S. Chen, D. C. W. Tsang and J. P. Tessonnier, *Appl. Catal., B*, 2020, **261**, 118126.
9 Y. Román-Leshkov, M. Moliner, J. A. Labinger and M. E. Davis, *Angew. Chem., Int. Ed.*, 2010, **49**, 8954–8957.
10 Q. Guo, L. Ren, P. Kumar, V. J. Cybulskis, K. A. Mkhoyan, M. E. Davis and M. Tsapatsis, *Angew. Chem., Int. Ed.*, 2018, **57**, 4926–4930.
11 Y. N. Palai, A. Shrotri, M. Asakawa and A. Fukuoka, *Catal. Today*, 2021, **365**, 241–248.
12 J. W. Harris, M. J. Cordon, J. R. Di Iorio, J. C. Vega-Vila, F. H. Ribeiro and R. Gounder, *J. Catal.*, 2016, **335**, 141–154.
13 H. Nguyen, V. Nikolakis and D. G. Vlachos, *ACS Catal.*, 2016, **6**, 1497–1504.
14 H. Zhao, J. E. Holladay, H. Brown and Z. C. Zhang, *Science*, 2007, **316**, 1597–1600.
15 S. Hu, Z. Zhang, J. Song, Y. Zhou and B. Han, *Green Chem.*, 2009, **11**, 1746–1749.

16 V. Choudhary, S. H. Mushrif, C. Ho, A. Anderko, V. Nikolakis, N. S. Marinkovic, A. I. Frenkel, S. I. Sandler and D. G. Vlachos, *J. Am. Chem. Soc.*, 2013, **135**, 3997–4006.
17 R. Gounder and M. E. Davis, *J. Catal.*, 2013, **308**, 176–188.
18 Y. P. Li, M. Head-Gordon and A. T. Bell, *ACS Catal.*, 2014, **4**, 1537–1545.
19 S. Ribeiro, A. D. S. S. Barbosa, A. C. Gomes, M. Pillinger, I. S. Gonçalves, L. Cunha-Silva and S. S. Balula, *Fuel Process. Technol.*, 2013, **116**, 350–357.
20 D. Julião, A. C. Gomes, M. Pillinger, L. Cunha-Silva, B. De Castro, I. S. Gonçalves and S. S. Balula, *Fuel Process. Technol.*, 2015, **131**, 78–86.
21 V. K. Abdelkader-Fernández, D. M. Fernandes, S. S. Balula, L. Cunha-Silva, M. J. Pérez-Mendoza, F. J. López-Garzón, M. F. Pereira and C. Freire, *ACS Appl. Energy Mater.*, 2019, **2**, 1854–1867.
22 C. Freire, D. M. Fernandes, M. Nunes and V. K. Abdelkader, *ChemCatChem*, 2018, **10**, 1703–1730.
23 V. K. Abdelkader-Fernández, D. M. Fernandes, S. S. Balula, L. Cunha-Silva and C. Freire, *J. Mater. Chem. A*, 2020, **8**, 13509–13521.
24 V. K. Abdelkader-Fernández, D. M. Fernandes, S. S. Balula, L. Cunha-Silva and C. Freire, *ACS Appl. Energy Mater.*, 2020, **3**, 2925–2934.
25 A. Kirchon, L. Feng, H. F. Drake, E. A. Joseph and H. C. Zhou, *Chem. Soc. Rev.*, 2018, **47**, 8611–8638.
26 S. Yuan, L. Feng, K. Wang, J. Pang, M. Bosch, C. Lollar, Y. Sun, J. Qin, X. Yang, P. Zhang, Q. Wang, L. Zou, Y. Zhang, L. Zhang, Y. Fang, J. Li and H. C. Zhou, *Adv. Mater.*, 2018, **30**, 1704303.
27 J. N. Hall and P. Bollini, *ACS Catal.*, 2020, **10**, 3750–3763.
28 R. Fang, A. Dhakshinamoorthy, Y. Li and H. Garcia, *Chem. Soc. Rev.*, 2020, **49**, 3638–3687.
29 A. E. R. S. Khder, H. M. A. Hassan and M. S. El-Shall, *Appl. Catal., A*, 2014, **487**, 110–118.
30 H. M. A. Hassan, M. A. Betiha, S. K. Mohamed, E. A. El-Sharkawy and E. A. Ahmed, *J. Mol. Liq.*, 2017, **236**, 385–394.
31 H. M. A. Hassan, M. A. Betiha, S. K. Mohamed, E. A. El-Sharkawy and E. A. Ahmed, *Appl. Surf. Sci.*, 2017, **412**, 394–404.
32 M. S. El-Shall, V. Abdelsayed, A. E. R. S. Khder, H. M. A. Hassan, H. M. El-Kaderi and T. E. Reich, *J. Mater. Chem.*, 2009, **19**, 7625–7631.
33 G. Akiyama, R. Matsuda, H. Sato and S. Kitagawa, *Chem.–Asian J.*, 2014, **9**, 2772–2777.
34 Q. X. Luo, Y. B. Zhang, L. Qi and S. L. Scott, *ChemCatChem*, 2019, **11**, 1903–1909.
35 S. Rojas-Buzo, A. Corma, M. Boronat and M. Moliner, *ACS Sustainable Chem. Eng.*, 2020, **8**, 16143–16155.
36 Y. Su, G. Chang, Z. Zhang, H. Xing, B. Su, Q. Yang, Q. Ren, Y. Yang and Z. Bao, *AIChE J.*, 2016, **62**, 4403–4417.
37 M. Yabushita, P. Li, T. Islamoglu, H. Kobayashi, A. Fukuoka, O. K. Farha and A. Katz, *Ind. Eng. Chem. Res.*, 2017, **56**, 7141–7148.
38 R. Oozeerally, D. L. Burnett, T. W. Chamberlain, R. I. Walton and V. Degirmenci, *ChemCatChem*, 2018, **10**, 706–709.
39 R. Oozeerally, S. D. K. Ramkhelawan, D. L. Burnett, C. H. L. Tempelman and V. Degirmenci, *Catalysts*, 2019, **9**, 812.
40 V. Choudhary, A. B. Pinar, R. F. Lobo, D. G. Vlachos and S. I. Sandler, *ChemSusChem*, 2013, **6**, 2369–2376.
41 W. Deng, Q. Zhang and Y. Wang, *Catal. Today*, 2014, **234**, 31–41.
42 E. A. Pidko, V. Degirmenci, R. A. Van Santen and E. J. M. Hensen, *Angew. Chem., Int. Ed.*, 2010, **49**, 2530–2534.
43 B. Song, Z. Wu, Y. Yu and H. Wu, *Ind. Eng. Chem. Res.*, 2020, **59**, 7336–7345.
44 L. Han, J. Zhang, Y. Mao, W. Zhou, W. Xu and Y. Sun, *Ind. Eng. Chem. Res.*, 2019, **58**, 15489–15496.
45 W. Xu, G. Li, W. Li and H. Zhang, *RSC Adv.*, 2016, **6**, 37530–37534.
46 C. Férey, C. Mellot-Draznieks, C. Serre, F. Millange, J. Dutour, S. Surblé and I. Margiolaki, *Science*, 2005, **309**, 2040–2042.
47 F. Millange, C. Serre and G. Férey, *Chem. Commun.*, 2002, **2**, 822–823.
48 A. M. P. Peedikakkal and I. H. Aljundi, *ACS Omega*, 2020, **5**, 28493–28499.
49 L. Sciortino, A. Alessi, F. Messina, G. Buscarino and F. M. Gelardi, *J. Phys. Chem. C*, 2015, **119**, 7826–7830.
50 S. Bhattacharjee, C. Chen and W. S. Ahn, *RSC Adv.*, 2014, **4**, 52500–52525.
51 M. Meilikhov, K. Yusenko and R. Fischer, *Dalton Trans.*, 2009, 600–602.
52 Q. Liu, L. Ning, S. Zheng, M. Tao, Y. Shi and Y. He, *Sci. Rep.*, 2013, **3**, 1–6.
53 N. R. Dhumal, M. P. Singh, J. A. Anderson, J. Kiefer and H. J. Kim, *J. Phys. Chem. C*, 2016, **120**, 3295–3304.
54 F. Dorosti and A. Alizadehdakhel, *Chem. Eng. Res. Des.*, 2018, **136**, 119–128.
55 X. Huang, Q. Hu, L. Gao, Q. Hao, P. Wang and D. Qin, *RSC Adv.*, 2018, **8**, 27623–27630.
56 A. E. J. Hoffman, L. Vanduyfhuys, I. Nevjestić, J. Wieme, S. M. J. Rogge, H. Depauw, P. Van Der Voort, H. Vrielinck and V. Van Speybroeck, *J. Phys. Chem. C*, 2018, **122**, 2734–2746.
57 H. Li, M. Eddaoudi, M. O'Keeffe and O. M. Yaghi, *Nature*, 1999, **402**, 276–279.
58 J. I. Feldblyum, M. Liu, D. W. Gidley and A. J. Matzger, *J. Am. Chem. Soc.*, 2011, **133**, 18257–18263.
59 A. Dhakshinamoorthy, M. Alvaro, P. Horcajada, E. Gibson, M. Vishnuvarthan, A. Vimont, J.-M. Grenèche, C. Serre, M. Daturi and H. Garcia, *ACS Catal.*, 2012, **2**, 2060–2065.
60 Z.-D. Tan, H.-Y. Tan, X.-Y. Shi, Z. Ji, Y.-F. Yan and Y. Zhou, *Inorg. Chem. Commun.*, 2015, **61**, 128–131.
61 A. Henschel, K. Gedrich, R. Kraehnert and S. Kaskel, *Chem. Commun.*, 2008, 4192–4194.
62 A. Maleki, B. Hayati, M. Naghizadeh and S. Joo, *J. Ind. Eng. Chem.*, 2015, **28**, 211–216.
63 X.-X. Huang, L.-G. Qiu, W. Zhang, Y.-P. Yuan, X. Jiang, A.-J. Xie, Y.-H. Shen and J.-F. Zhu, *CrystEngComm*, 2012, **14**, 1613–1617.

64 A. Vishnyakov, P. I. Ravikovitch, A. V. Neimark, M. Bülow and Q. M. Wang, *Nano Lett.*, 2003, **3**, 713–718.
65 D. T. Sun, L. Peng, W. S. Reeder, S. M. Moosavi, D. Tiana, D. K. Britt, E. Oveisi and W. L. Queen, *ACS Cent. Sci.*, 2018, **4**, 349–356.
66 S. Nießing and C. Janiak, *Mol. Catal.*, 2019, **467**, 70–77.
67 L. Yang, W. Liu, Z. Zhang, X. Du, J. Gong, L. Dong and Y. Deng, *Electrochim. Acta*, 2017, **246**, 1163–1173.
68 Y. Zhang, E. A. Pidko and E. J. M. Hensen, *Chem.–Eur. J.*, 2011, **17**, 5281–5288.
69 P. Wrigstedt, J. Keskiväli, M. Leskelä and T. Repo, *ChemCatChem*, 2015, **7**, 501–507.